MOLECULAR ONCOLOGY 9 (2015) 527–543

available at www.sciencedirect.com

ScienceDirect

www.elsevier.com/locate/molonc

Oncogenic signaling in amphiregulin and EGFR-expressing PTEN-null human breast cancer

Christiana S. Kappler[a,*,1], Stephen T. Guest[a,1], Jonathan C. Irish[a], Elizabeth Garrett-Mayer[b], Zachary Kratche[a], Robert C. Wilson[a], Stephen P. Ethier[a]

[a]Department of Pathology and Laboratory Medicine, Hollings Cancer Center, Medical University of South Carolina, Charleston, SC 29425, USA
[b]Department of Public Health Science, Medical University of South Carolina, Charleston, SC 29425, USA

ARTICLE INFO

Article history:
Received 23 September 2014
Received in revised form
15 October 2014
Accepted 17 October 2014
Available online 23 October 2014

Keywords:
Triple-negative breast cancer
Epidermal growth factor receptor
PTEN
shRNA screen

ABSTRACT

A subset of triple negative breast cancer (TNBC) is characterized by overexpression of the epidermal growth factor receptor (EGFR) and loss of PTEN, and patients with these determinants have a poor prognosis. We used cell line models of EGFR-positive/PTEN null TNBC to elucidate the signaling networks that drive the malignant features of these cells and cause resistance to EGFR inhibitors. In these cells, amphiregulin (AREG)-mediated activation of EGFR results in up-regulation of fibronectin (FN1), which is known to be a mediator of invasive capacity via interaction with integrin β1. EGFR activity in this PTEN null background also results in Wnt/beta-catenin signaling and activation of NF-κB. In addition, AKT is constitutively phosphorylated in these cells and is resistant to gefitinib. Expression profiling demonstrated that AREG-activated EGFR regulates gene expression differently than EGF-activated EGFR, and functional analysis via genome-scale shRNA screening identified a set of genes, including PLK1 and BIRC5, that are essential for survival of SUM-149 cells, but are uncoupled from EGFR signaling. Thus, our results demonstrate that in cells with constitutive EGFR activation and PTEN loss, critical survival genes are uncoupled from regulation by EGFR, which likely mediates resistance to EGFR inhibitors.

© 2014 The Authors. Published by Elsevier B.V. on behalf of Federation of European Biochemical Societies. This is an open access article under the CC BY-NC-ND license (http://creativecommons.org/licenses/by-nc-nd/3.0/).

1. Introduction

Triple negative breast cancers, while making up a relatively small fraction of all breast cancers, are responsible for a disproportionate share of breast cancer deaths (Prat and Perou, 2011). With the advent of taxane-based chemotherapies, many patients with TNBC respond to cytotoxic chemotherapies (Schneider et al., 2008). In the neoadjuvant setting, however, pathological complete response rates for TNBC are still substantially below 50%, and patients who have a poor response to neoadjuvant chemotherapy have poor outcomes (Lehmann et al., 2011; Masuda et al., 2013). Thus, the response of TNBC to neoadjuvant chemotherapy is a biomarker of the intrinsic sensitivity or resistance of breast cancer cells to cytotoxic chemotherapy.

* *Corresponding author*. Department of Pathology and Laboratory Medicine, Medical University of South Carolina, 68 President Street, Room 431, Charleston, SC 29425, USA. Tel.: +1 8432243674.
E-mail address: kapplerc@musc.edu (C.S. Kappler).
[1] These authors contributed equally to this work.
http://dx.doi.org/10.1016/j.molonc.2014.10.006
1574-7891/© 2014 The Authors. Published by Elsevier B.V. on behalf of Federation of European Biochemical Societies. This is an open access article under the CC BY-NC-ND license (http://creativecommons.org/licenses/by-nc-nd/3.0/).

To improve the therapeutic response of TNBC patients, a number of laboratory and clinical studies have been aimed at identifying novel targeted therapeutic approaches for the treatment of this subset of patients. The most likely target in this setting is the epidermal growth factor receptor (EGFR), which is overexpressed in the majority of TNBCs (Masuda et al., 2013; Harris et al., 1989; Nicholson et al., 1989, 1990, 1991). However, attempts to employ EGFR-targeted agents have met with limited success (Agrawal et al., 2005; Pal et al., 2011). Thus, there remains a pressing need to develop novel targeted therapeutic strategies for the treatment of TNBC.

Our laboratory has developed a number of cell line models of TNBC, including the SUM-149, SUM-229, SUM-102, SUM-159, and SUM-1315 cell lines (Ethier et al., 1993, 1996; Ethier, 1996; Forozan et al., 1999; Woods Ignatoski and Ethier, 1999). Among these cell lines, SUM-159 and SUM-1315 cells have been recently demonstrated to be models of the claudin-low subset of TNBCs (Prat et al., 2013). By contrast, SUM-149 and SUM-229 cells are good models of aggressive TNBC and have molecular profiles similar to those of TNBC patients that exhibit a poor response to neoadjuvant chemotherapy (Lehmann et al., 2011). Previously, we demonstrated that SUM-149 cells require EGFR signaling for growth, and that constitutive activation of EGFR in these cells is the result of an amphiregulin (AREG)-mediated autocrine loop (Rao et al., 2000; Berquin et al., 2001). We also reported that AREG alters the biology of the EGFR, resulting in increased stability of the receptor and its accumulation at the cell surface (Willmarth et al., 2008). This cell surface-localized constitutively active EGFR then drives inflammatory and anti-apoptotic pathways mediated by IL1 and NF-κB (Streicher et al., 2007). More recently, we demonstrated the importance of this autocrine loop in mediating the invasive characteristics of TNBC cells (Baillo et al., 2011).

Studies published in 2009 showed that SUM-149 cells are PTEN null as a result of an intergenic deletion that blocks mRNA synthesis of PTEN but does not alter the coding sequence of the gene (Saal et al., 2008). Interestingly, SUM-229 cells also express high levels of AREG resulting in constitutive EGFR activation, and are also PTEN null (unpublished observations). These two cell lines are similar to a third, commonly used TNBC cell line, MDA-MB-468, which has an EGFR amplification and are also PTEN null (Buick et al., 1990). Recently, Martin, et al. (Martin et al., 2012) demonstrated that EGFR overexpression and PTEN loss is common in TNBCs, with approximately 75% of cases exhibiting one of these molecular alterations. Further, they showed that PTEN loss in the context of EGFR overexpression occurs in approximately 40% of cases. More recent data published by Masuda et al. (Masuda et al., 2013) demonstrated that this combination of genomic alterations results in aggressive disease, with few if any patients having a complete pathologic response to neoadjuvant chemotherapy. Thus, overexpression of cell surface EGFR in association with PTEN loss is a common combination in an aggressive and drug-resistant subset of TNBC.

In the present studies, we demonstrate that AREG-activated EGFR, in the context of PTEN loss, results in the activation of an oncogenic signaling network that drives many aspects of the malignant potential of the cells and may also influence intrinsic drug resistance. We report here that AREG-mediated EGFR activation by itself is sufficient to induce up-regulation of FN1 at the message and protein level. We have reported previously on the importance of FN1-mediated integrin signaling in breast cancer cell motility and invasion (Jia et al., 2004), and activation of this signaling axis by AREG likely explains how AREG/EGFR signaling influences the motility and invasive capacity of these cells. The loss of PTEN in SUM-149 cells results in increased AKT expression and a dramatic increase in AKT phosphorylation at both pT308 and pS473. Using several omics strategies, including reverse phase protein arrays, RNA Seq, and genome-scale shRNA screening, we found that in this oncogenic signaling network, the regulation of key survival genes becomes uncoupled from EGFR signaling. We propose that this uncoupling plays a role in the survival of TNBC cells exposed to EGFR inhibitors. This may explain why EGFR inhibitors have been relatively ineffective in the treatment of TNBC. The elucidation of this network will allow us to make predictions regarding targeted combinatorial strategies that could prove effective in TNBC cells with a similar molecular signature.

2. Materials and methods

2.1. Cell culture

SUM-149 cells were maintained in Ham's F-12 medium with 5% fetal bovine serum, 5 μg/ml insulin, 2 μg/ml hydrocortisone, 5 μg/ml gentamicin, and 2.5 μg/ml fungizone (5%IH). MCF10A + EGF and MCF10A + AREG cells were maintained in SFIH (Ham's F-12 with 1 μg/ml hydrocortisone, 1 mg/ml bovine serum albumin, 10 mM HEPES, 5 mM ethanolamine, 5 μg/ml transferrin, 10 nM triiodothyronine, 50 nm sodium selenate, 25 μg/ml gentamicin, 2.5 μg/ml fungizone, and 5 μg/ml insulin) with 10 ng/ml EGF (SFIHE) or 20 ng/ml AREG (SFIHA), respectively. SUM-229 cells were maintained in 5% IH, and MDA-MB-468 cells were maintained in DMEM with 10% fetal bovine serum, 5 μg/ml gentamicin, and 2.5 μg/ml fungizone. All cells were maintained in a humidified incubator at 37 °C and 10% CO_2. AREG knockdown cells were generated as described previously, and were maintained in 5%IH with 1 μg/ml puromycin (Baillo et al., 2011).

2.2. Western blotting

Cells were plated and grown to 90% confluency. Where indicated, the cells were treated with 0.5 μM gefitinib for the indicated times. Cells were then lysed in a buffer containing 20 mM Tris–HCl (pH 8.0), 137 mM NaCl, 1% NP40, 10% glycerol, 1 mM Na_3VO_4, and 1× Protease Inhibitor cocktail (Calbiochem, 539131), and protein concentrations were measured by Bradford assay (Bio-Rad). Laemmli sample buffer was added to the lysates and the samples were boiled for 5 min before being separated by electrophoresis on SDS-polyacrylamide gels (Bio-Rad). After transferring the proteins to polyvinylidene difluoride (PVDF) membranes, blots were probed overnight at 4 °C with the indicated antibodies: PTEN (1:1000; Cell Signaling #9188), FN1 (1:5000; Abcam ab32419), PathScan Multiplex Western Cocktail (1:500; Cell Signaling #5301).

2.3. Wnt reporter constructs

Stable expression of Wnt reporter constructs was performed using Mission Lentiviral Packaging Mix (Sigma, SHP001). Plasmid 24305 (7TGP) encoding seven repeats of the Wnt TCF/LEF binding sequence upstream of a GFP reporter, as well as a puromycin selection marker, was obtained from Addgene (Fuerer and Nusse, 2010). To produce lentivirus, HEK293 cells at 80% confluence were transfected in 10% DMEM (without antibiotics) with 3 μg of the construct and the packaging mix using Lipofectamine 2000 according to the manufacturer's protocol. Cells were incubated for 12–14 h at 37 °C, at which time media was changed to 10% DMEM with antibiotics. Virus was harvested at 48 and 72 h post-infection, centrifuged at 1500 rpm for 5 min and filtered through a 0.45 micron filter. Recipient cells were seeded at 1×10^6 cells per 10 cm dish, allowed to adhere overnight and then treated with 8 μg/ml polybrene and infected. Cells were incubated for 12 h and new media was added. After 2–3 days, 1 μg/ml puromycin was added to select for cells expressing the reporter construct. Cells were maintained for 2 weeks before functional assays were performed.

2.4. In vitro mammosphere assays

Cells were plated in ultra-low attachment plates (Corning Inc., Acton, MA, USA) at a density of 10,000 cells/well in serum-free mammary epithelial growth medium (MEBM Basal Medium, Lonza, Walkersville, MD, USA) supplemented with B27 (Invitrogen, Carlsbad, CA, USA), basic FGF (20 ng/ml), heparin (4 μg/ml), and epidermal growth factor (20 ng/ml). Fresh medium (1 ml) was added every three days and the cells were cultured for 7–10 days, at which point images of representative mammospheres were captured using an EVOS FL Auto Cell Imaging System. The mammospheres were then harvested, dissociated by trypsinization, and the cells were analyzed by flow cytometry for GFP expression. Gating for flow cytometry analysis was established using non-transfected SUM-149 cells as a negative control.

2.5. Cell proliferation assays

Cells were seeded on day 0 in 6-well plates at 35,000 cells/well. After 7 days of treatment as indicated, plates were washed three times with PBS and agitated on a rocker table with 0.5 ml Hepes/$MgCl_2$ buffer (0.01 mM HEPES and 0.015 mM $MgCl_2$) for 5 min. Cells were then lysed for 10 min by the addition of a ethyl hexadecyldimethylammonium solution, and the nuclei were counted using a Z1 Coulter Counter (Beckman Coulter, Brea, CA, USA). Day 1 cells were counted for seeding efficiency. All experiments were performed in triplicate. To assess cell proliferation with different EGFR ligands, the following concentrations were used: EGF, 10 ng/ml; HB-EGF, 10 ng/ml and 50 ng/ml; epigen, 20 ng/ml; epiregulin, 20 ng/ml; amphiregulin, 20 ng/ml and TGF-α, 10 ng/ml. To determine the effect of inhibition of BIRC5 and PLK1 on cell growth and viability, YM155 (10 nM; Selleckchem S1130) and BI 2536 (25 nM; Selleckchem S1109) were used to inhibit the activity of BIRC5 and PLK1, respectively. Gefitinib (Selleckchem #S0125) was used at 0.5 μM.

2.6. RPPA analysis

For RPPA analysis, MCF10A + EGF, MCF10A + AREG and SUM-149 cells were grown to 90% confluency in 60-mm plates. Cells were treated with 0.5 μM gefitinib for 0, 30, 60, 90, or 120 min, as indicated. Each treatment condition was performed in duplicate. Cells were then lysed in 100 μl RPPA lysis buffer containing 1% Triton X-100, 50 mM HEPES, 150 mM NaCl, 1.5 mM $MgCl_2$, 1 mM EGTA, 100 mM sodium fluoride, 10 mM sodium pyrophosphate, 1 mM sodium orthovanadate, 10% glycerol and protease/phosphatase inhibitors (Roche #05056489001/04906837001). Protein concentrations were determined by Bradford assay (BioRad) and concentrations were adjusted to 1 μg/ml. The samples were then mixed with 4× SDS sample buffer containing 0.2 M Tris–HCl (pH 8.0), 40% glycerol and 8% SDS, boiled for 5 min, and stored at −80 °C until shipment to the RPPA Core Facility at MD Anderson for analysis.

2.7. RNA-Seq analysis

MCF10A + EGF, MCF10A + AREG and SUM-149 cells were grown to 90% confluency, and then treated with 500 nM gefitinib for 24 h, or placed in SFIH in the absence of ligand for 24 h. RNA was isolated using an RNEasy kit from Qiagen (Cat. #74106, Qiagen) and stored at −80 °C until use. RNA integrity was verified on an Agilent 2100 TapeStation (Agilent Technologies, Palo Alto, CA). 100–200 ng of total RNA was used to prepare RNA-Seq libraries using the TruSeq RNA Sample Prep kit following the protocol described by the manufacturer (Illumina, San Diego, CA). Sequencing was performed on an Illumina HiScanSQ. Analysis was performed by the CGM Bioinformatics Core at the Medical Universit of South Carolina. The resulting data was processed using the program Trimmomatic to remove adaptors and low QC sequences, and the sequences were then confirmed with FastQC and aligned to the human genome build HG19 using Tophat (Bowtie2; alignments >93%). The resulting SAM files were sorted, inputted into HTSeq and analyzed with DEseq2.

2.8. Genome-scale shRNA screen

Virus pools expressing shRNA constructs were prepared according to the Cellecta Pooled Lentiviral shRNA Libraries User Manual protocol (www.cellecta.com). HEK 293T cells were transfected with each of the three Cellecta library plasmid DNA pools (Human Modules 1–3) and the Cellecta Ready-to-Use Packaging Mix (Cat #CPCP-K2A). For each module, virus was titered and used to transduce 5×10^7 SUM-149 cells at an MOI of 0.5 in the presence of 5 μg/ml polybrene. Following transduction, cells were cultured for 3 days to allow expression of the resistance marker. Non-transduced cells were eliminated from the culture by the addition of 2 μg/ml puromycin to the growth media. Three days after the addition of puromycin, cells were trypsinized and one-half of the total population was harvested for genomic DNA preparation. This DNA served as the reference time point DNA. The remaining cells were plated and grown for approximately 7 population doublings before being harvested for genomic DNA preparation. Genomic DNA was prepared by phenol:chloroform

extraction according to the Cellecta Pooled Lentiviral shRNA Libraries User Manual protocol.

See Supplementary Methods for detailed descriptions of the shRNA screen and statistical analyses.

3. Results

3.1. EGFR-mediated cell signaling in AREG- and EGF-stimulated MCF-10A and SUM-149 cells

To begin to explore the basis for the oncogenic signaling network mediated by AREG and EGFR in our model cell lines, we studied the influence of AREG versus EGF activation of EGFR in MCF-10A cells and SUM-149 cells on proliferation, signaling properties, and gene expression.

Because AREG activates EGFR via an autocrine loop in SUM-149 cells, we used AREG knock-down versions of SUM-149 cells to examine the responsiveness of these cells to AREG (Figure 1A). AREG knock-down cells grew poorly under serum-free conditions in the absence of exogenous ligand, but were responsive to the proliferative effects of AREG and other EGF family members (Figure 1B). The data in Figure 1A shows that for MCF-10A cells, higher concentrations of AREG than EGF were required to generate the same level of proliferation ($P < 0.0001$). This is likely due to the lower affinity of AREG for EGFR, as has been reported previously (Johnson et al., 1993; Beerli and Hynes, 1996; Ma et al., 2001; Stern et al., 2008). By contrast, SUM-149 cells were responsive to both AREG and EGF. Because AREG is a heparin-binding growth factor, factors other than affinity for the receptor, such as the repertoire of heparin-sulfate proteoglycans on the cell surface, can influence the responsiveness of cells to AREG (Johnson and Wong, 1994; Narita et al., 2007). Of note, SUM-149 cells responded robustly to low levels of EGF, but this was followed by a decrease in proliferation at higher levels. Because SUM-149 express high levels of EGFR, these observations likely reflect the effects of excessive stimulation of EGFR in these cells and are in agreement with previous studies reporting decreased proliferation in response to high levels of EGF (Danielsen and Maihle, 2002).

To investigate the differences in cell signaling induced by AREG and EGF in MCF-10A and SUM-149 cells, we examined the expression and activation of key cell signaling proteins by western blot analysis using a multi-protein antibody cocktail (Figure 1C). The results of these experiments suggested that AREG is a weak activator of MEK/MAPK signaling compared to EGF, as MCF-10A cells stimulated with AREG, SUM-149 cells, SUM-229 cells (AREG-positive), and MDA-MB-468 cells (EGFR-amplified) exhibited low levels of phospho-p44/42 MAPK compared to EGF-stimulated MCF-10A cells. Despite these relatively low levels, phospho-MAPK was responsive to EGFR inhibition by gefitinib in all three cell lines (Figure 1D). AKT phosphorylation at pS473 was observed at low levels in MCF-10A cells regardless of the presence of EGF or AREG in the medium. By contrast, AKT phosphorylation at the serine 473 site was markedly elevated in SUM-149 cells compared to MCF-10A cells, and was insensitive to EGFR inhibition with gefitinib. A similar increase in AKT pS473 was observed in SUM-229 cells and MDA-MB-468 cells. Thus, not surprisingly, in the three PTEN null cell lines with constitutively active EGFR, AKT phosphorylation was high, but not regulated by EGFR signaling.

3.2. RPPA analysis of signaling pathways in SUM-149 and MCF-10A cells

To gain further insight into the differential signaling properties of AREG-versus EGF-stimulated EGFR in MCF-10A and SUM-149 cells, we performed experiments using reverse phase protein arrays (RPPAs). In these experiments, cell lysates were prepared from SUM-149 cells or MCF-10A cells cultured in media containing EGF or AREG and examined via RPPA. As part of the experiment, we also measured the influence of gefitinib on the expression and phosphorylation of the proteins on the array. The overall results of this experiment are summarized in the heat map shown in Supplementary Figure 1.

3.2.1. Amphiregulin-specific signaling

To identify signaling changes that were specifically associated with AREG-mediated EGFR signaling versus EGF-mediated signaling, we looked for similarities in the expression or activation of proteins in MCF-10A + AREG and SUM-149 cells compared to MCF-10A + EGF cells. As shown in Figure 2A, the expression levels of several proteins and phosphoproteins were higher in both MCF-10A + AREG and SUM-149 cells compared to MCF-10A + EGF cells, including EGFR and EGFR-pY1068, FN1, FASN, GAB2, src and src-pY527, and STAT3 pY705 (*$P < 0.05$ by t-test compared to MCF-10A + EGF at time = 0; †$P < 0.001$ by ANOVA of time series compared to MCF-10A + EGF). The changes in EGFR protein expression observed in these experiments are in keeping with our previous observations on the ability of AREG to stabilize EGFR, resulting in overexpression at the protein level (Willmarth et al., 2008; Willmarth and Ethier, 2006). Of note, AREG-mediated EGFR activation resulted in dramatically elevated levels of FN1. This increase in FN1 expression was striking and was confirmed at both the protein level by western blot and the message level by RNA-Seq (Figure 2B). High level FN1 expression in AREG-stimulated cells (including SUM-229) is also consistent with our previous findings on the role of AREG in mediating cell motility and invasion (Baillo et al., 2011; Willmarth and Ethier, 2006).

In addition to the higher levels of protein expression and phosphorylation observed in AREG-stimulated MCF-10A cells and SUM-149 cells compared to MCF-10A + EGF cells, several proteins exhibited lower levels of expression and phosphorylation, and nearly all of these were mTOR-associated proteins. As shown in Figure 2C, the overall levels of 4EBP-1 and 4EBP-1 pS65/pT37, p70S6K (SUM-149 only) and p70S6K pT389, S6 and S6 pT235/pT240, Rictor, mTOR pS2448, and PRAS40 were significantly lower in both MCF-10A + AREG cells and SUM-149 cells compared to MCF-10A + EGF cells (*$P < 0.05$ by t-test compared to MCF-10A + EGF at time = 0; †$P < 0.001$ by ANOVA of time series compared to MCF-10A + EGF). These findings are in agreement with our observation of low levels of phosphorylation of S6 protein, which is a downstream target of mTORC1, in SUM-149 cells (Figure 1C).

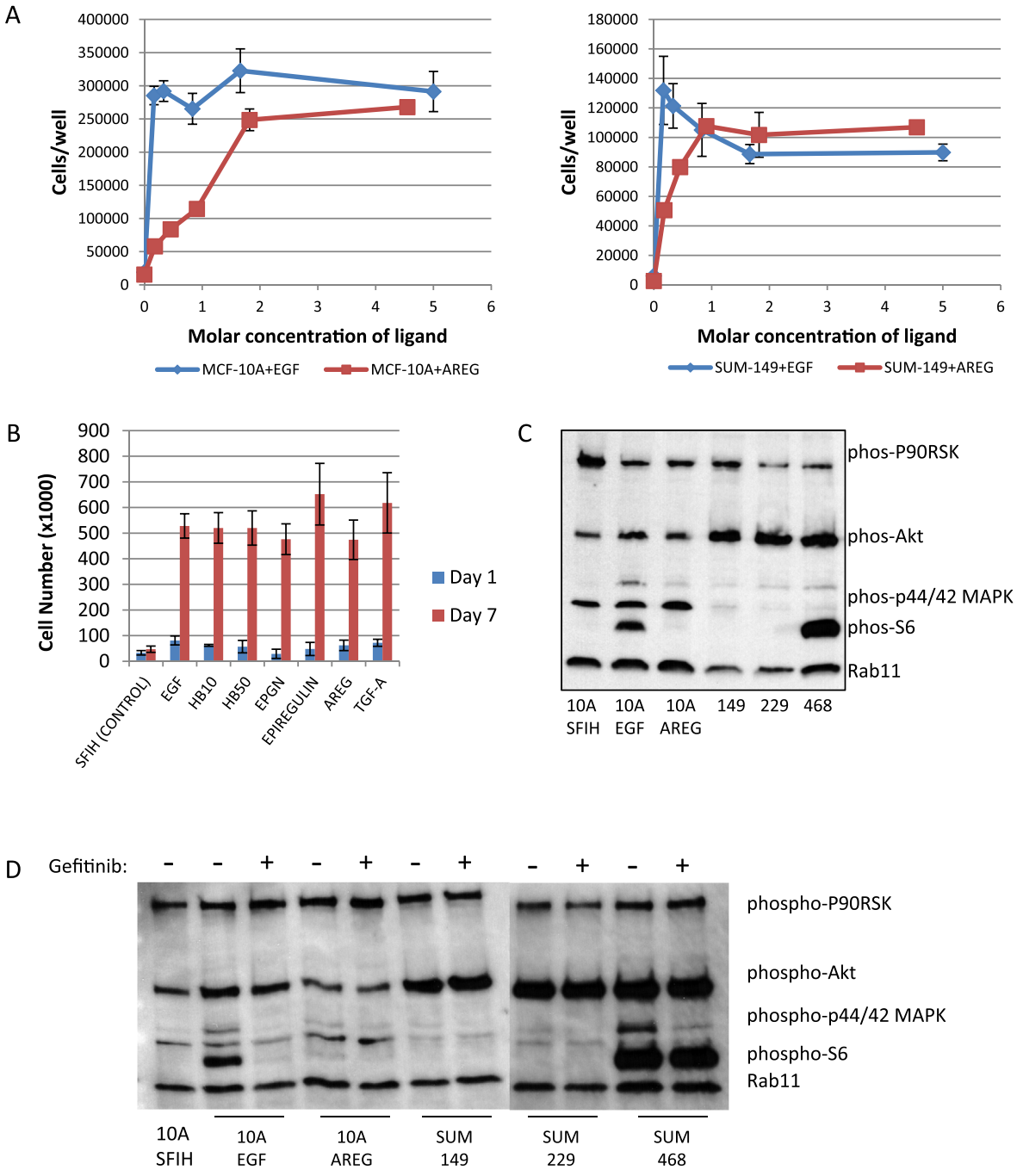

Figure 1 – Differential effects of AREG and EGF in MCF-10A and SUM-149 cells. A. Cells were grown for 7 days in media containing EGF or AREG and counted. Values are the mean ± standard deviation of triplicate wells. $P < 0.0001$ for EGF vs. AREG in SUM149 cells; $P < 0.0001$ for EGF vs. AREG in MCF10A cells. B. SUM-149 AREG knock-down cells were grown for 7 days in serum-free media (SFIH) containing the following EGFR ligands, as indicated: EGF (10 ng/ml), HB-EGF (HB10, 10 ng/ml; HB50,50 ng/ml), epigen (EPGN, 20 ng/ml), epiregulin (20 ng/ml), amphiregulin (AREG, 20 ng/ml) and TGF-α (TGF-A, 10 ng/ml). C. Western blot of signaling proteins in MCF-10A cells grown in SFIH alone or in the presence of EGF (10 ng/ml) or AREG (20 ng/ml), SUM-149, SUM-229 and MDA-MB-468 cells. D. Effect of EGFR inhibition on signaling proteins in MCF-10A and SUM-149 cells. Cells were exposed to 0.5 μM gefitinib for 60 min and the phosphorylation state of signaling proteins was assessed by Western blot. A sample from MCF-10A cells grown in SFIH alone is included for reference.

3.2.2. *SUM-149-specific signaling*

The RPPA data also revealed several changes specific for SUM-149 cells (Figure 2D; †$P < 0.001$ by ANOVA of time series compared to MCF-10A + EGF; ‡$P < 0.001$ by ANOVA of time series compared to MCF-10A + AREG). The most striking was the complete absence of PTEN in SUM-149 cells. This was not unexpected, since we have published previously that SUM-149 cells have a micro-deletion within the PTEN gene

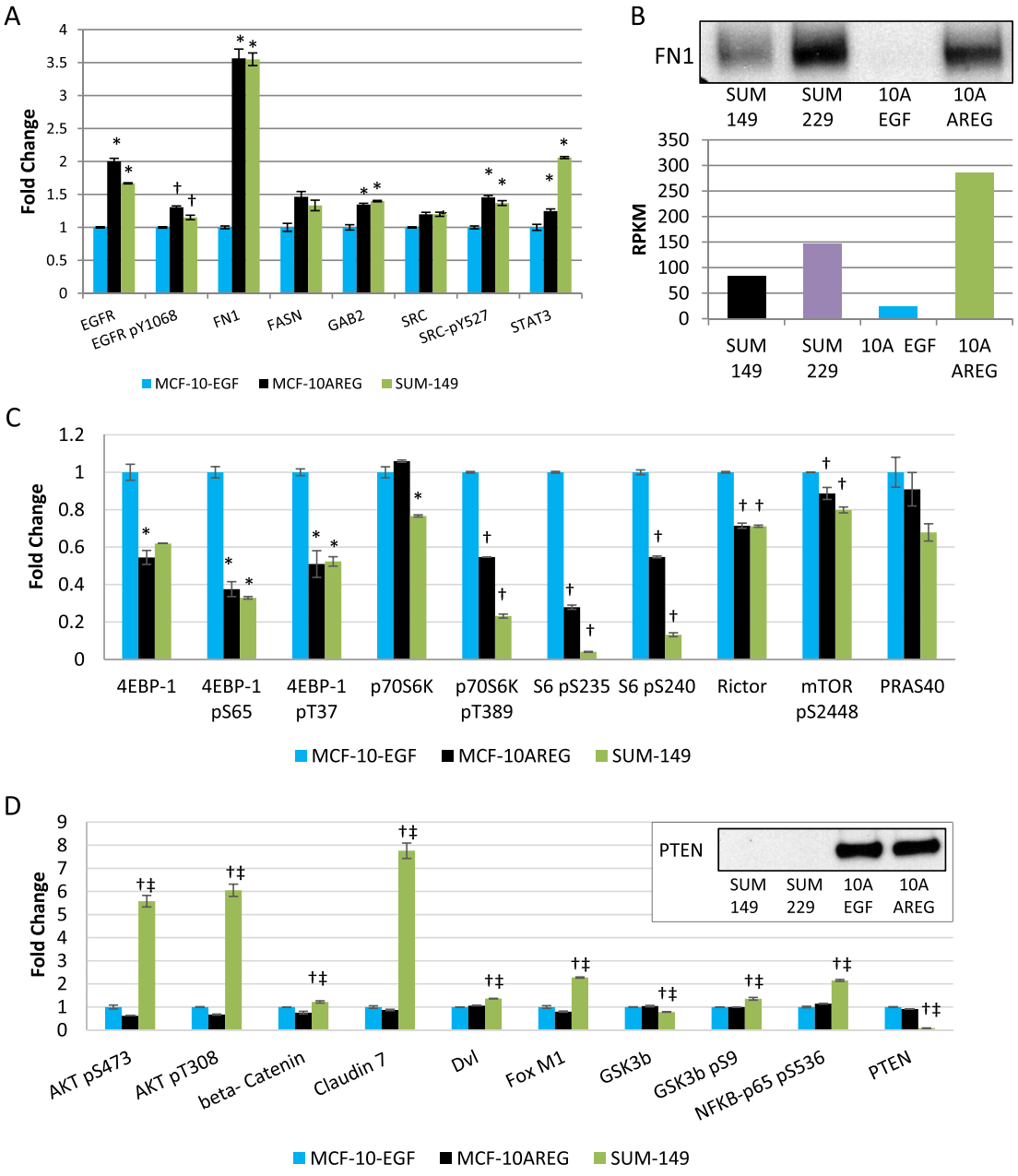

Figure 2 – RPPA and Western blot analysis of changes in signaling proteins in MCF-10 + AREG and SUM-149 cells compared to MCF-10A + EGF cells. Data were normalized to MCF-10 + EGF values, and the error bars indicate the standard deviation from the mean from duplicate plates. Significance is indicated as follows: *$P < 0.05$ by *t*-test compared to MCF-10A + EGF at time = 0; †$P < 0.001$ by ANOVA of time series compared to MCF-10A + EGF; ‡$P < 0.001$ by ANOVA of time series compared to MCF-10A + AREG. A. RPPA analysis of proteins and phospho-proteins increased in MCF-10A + AREG and SUM-149 cells compared to MCF-10A + EGF cells. B. Western blot (upper) and RNA-Seq (bar graph, lower) analysis of fibronectin (FN1) protein and mRNA expression, respectively, in MCF-10A, SUM-149 and SUM-229 cells, as indicated. C. RPPA analysis of proteins and phospho-proteins decreased in MCF-10A + AREG and SUM-149 cells compared to MCF-10A + EGF cells. D. RPPA analysis of proteins and phospho-proteins increased in SUM-149 cells only. Inset shows Western blot analysis of PTEN expression in SUM-149, SUM-229, MCF-10A + EGF and MCF-10A + AREG cells.

that results in loss of expression at the mRNA level (Saal et al., 2008). Expression profiling confirmed a lack of PTEN expression at the mRNA level, and no PTEN was detected in these cells by western blot analysis (Figure 2D). In keeping with the loss of PTEN in SUM-149 cells, we observed markedly higher levels of AKT phosphorylation at the pT308 and pS473 sites.

We reported previously that in SUM-149 cells, autocrine signaling loops induced by AREG-mediated EGFR activation result in expression of IL-1α and activation of NF-κB

(Streicher et al., 2007). The results obtained in the RPPA analysis are consistent with these earlier findings and confirm that levels NF-κB-p65 pS536 are higher in SUM-149 cells compared to MCF-10A + EGF or MCF-10A + AREG cells (Figure 2D). In addition, the RPPA experiments identified two other proteins dramatically increased in SUM-149 cells; claudin-7 and FoxM1 (Figure 2D and Supplementary Figure 2). The RPPA data indicate an approximately 2.2-fold increase in FoxM1 expression in SUM-149 cells compared to MCF-10A cells, and RNA-Seq analysis showed a 4-fold increase in FoxM1 mRNA expression in SUM-149 cells compared to MCF-10A cells (data not shown). With regard to claudin-7, RNA-Seq data indicated a 2-fold overexpression in SUM-149 cells versus MCF-10A cells (not shown), and the RPPA data show an approximate 8-fold increase at the protein level. Importantly, overexpression of both of these proteins has been associated with aggressive types of cancer (Katoh et al., 2013; Dahiya et al., 2011; Ding et al., 2013; Yang et al., 2013).

Figures 2D and 3A show additional differences in the expression and activation of signaling molecules specific to SUM-149 cells. Several proteins that are part of the canonical Wnt/beta-catenin pathway were altered in a SUM-149 cell-specific manner, including higher levels of Dvl expression, lower levels of GSK3β expression with higher levels of GSK3β S-9 phosphorylation, and higher levels of beta-catenin protein (†$P < 0.001$ compared to MCF-10A + EGF; ‡$P < 0.001$ compared to MCF-10A + AREG). When considered in conjunction with our previously published findings that AREG-mediated EGFR activation results in down-regulation of the Wnt pathway inhibitor DKK1 (Baillo et al., 2011), these results predict that SUM-149 cells are poised to activate Wnt/beta-catenin signaling. Based on these and our previous findings, we designed experiments to assess Wnt pathway activity in SUM-149 cells using Wnt reporter constructs. In previous experiments, we were unable to detect evidence of Wnt signaling activity in SUM-149 cells. We reasoned that the difficulty in detecting Wnt signaling in these cells might be because only a small fraction of cells in the population are actively signaling via this pathway at any given time, and/or that there is little Wnt pathway activity when the cells are maintained in monolayer culture. To address these possibilities, we stably transduced SUM-149 cells with a TCF/LEF lentiviral vector in which GFP activity is driven by a seven copy repeat of the TCF/LEF binding sequence (Fuerer and Nusse, 2010). This approach allowed us to develop SUM-149 cells stably expressing the Wnt reporter and examine Wnt activity in individual cells. In keeping with our previous results, we found that Wnt-driven GFP expression was detectable in only a very small number of SUM-149 cells per plate when grown in monolayer culture (Figure 3B). However, when SUM-149 cells were cultured in low-attachment plates in stem cell media, we observed clusters of cells with intense GFP expression within the mammospheres/anchorage-independent colonies (Figure 3C). FACS analysis of the cells confirmed that while little to no GFP was expressed in cells grown in 2D culture, cells grown in mammosphere culture conditions exhibited an increase in the proportion of cells expressing GFP, with GFP levels 100–1000-fold higher than that observed in 2D culture. These results indicate that a subset of SUM-149 cells is indeed poised to activate Wnt/beta-catenin signaling, and that this signaling activity is markedly increased when the cells are cultured under anchorage-independent conditions.

3.2.3. *EGFR-mediated signaling*

As a part of these RPPA experiments, we examined the influence of EGFR activity on the expression of signaling proteins in gefitinib-treated MCF-10A + EGF, MCF-10A + AREG, and SUM-149 cells. As expected, EGFR inhibition resulted in prompt down-regulation of several signaling proteins, such as c-MYC (not in SUM-149 cells), c-Met pY1235, c-Raf pS338, EGFR pY1068, MAPK pT202/Y204, MEK pS217, mTOR pS2448, S6 pS235/236 and pS240/S244 and P70s6K pT389 (Figure 4). Many of these proteins, especially those belonging to MAPK signaling pathways, are known to contribute to the regulation of cell cycle progression and proliferation. In addition, they demonstrate that even though overall MAPK activity is lower in SUM-149 and MCF-10A + AREG cells than MCF-10A + EGF cells (Figure 1C), these pathways are still responsive to inhibition of EGFR (see also Figure 1D). These time course changes are shown in Figure 4, and were similar in all three cell lines/conditions. This is in contrast to the proteins described previously that were influenced in their steady-state levels specifically in SUM-149 cells, which were only slightly modulated by EGFR inhibition (Supplementary Figure 2). Statistical analysis of the proteins shown in Figure 4 and Supplementary Figure 2 are presented in Supplementary Table 5.

The overall results of the RPPA analysis are summarized in Figure 5. The results indicate that AREG-mediated stabilization of EGFR expression and activation induces a dramatic up-regulation of FN1, which may play a role in AKT activation in these cells. The data also show that EGFR activity in the context of PTEN loss results in high levels of AKT phosphorylation, which could prime the cells for Wnt/beta-catenin signaling and activation of NF-κB. Finally, the results also reveal significant reductions in the expression and activation of proteins in the mTORC1 pathway.

3.3. *Influence of AREG-mediated EGFR activation on gene expression in MCF-10A and SUM-149 cells*

To measure the influence of AREG versus EGF stimulation on gene expression, we performed RNA-Seq analysis on MCF-10A cells following continuous culture in medium containing either EGF or AREG. To identify the genes regulated by EGFR signaling in MCF-10A + EGF and MCF-10A + AREG, each cell line was exposed to 0.5 μM gefitinib for 24 h, and RNA was collected for RNA-Seq analysis. In addition, to confirm that the observed changes in gene expression following gefitinib treatment were specific to inhibition of EGFR, RNA-Seq was also performed on MCF-10A cells cultured for 24 h in the absence of exogenous EGF. Results of this analysis are shown in Supplementary Figure 3, and show that the gene expression profile resulting from inhibition of EGFR with gefitinib clustered closely with that produced by culture in EGF-free media. All RNA-Seq experiments were performed in duplicate and genes for which there were 10 reads or more with at least a 1.5 fold-change in expression, a *P*-value of less than 0.05, and an adjusted *P*-value of less than 0.1 based on

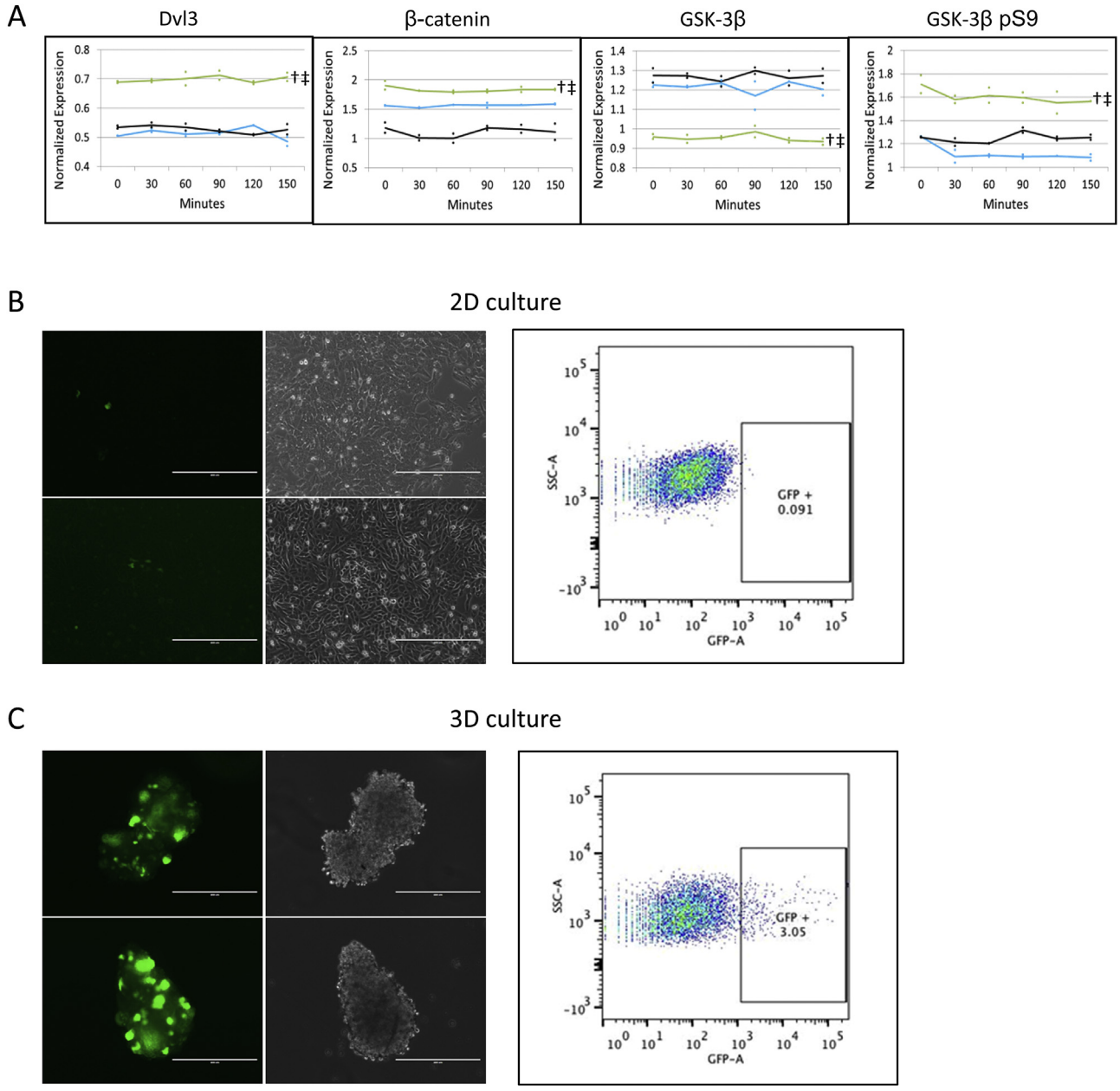

Figure 3 – Wnt/beta-catenin activity in SUM-149 cells. A. RPPA analysis of expression of Dvl3, β-catenin, GSK3β and phospho-GSK3β in the presence or absence of gefitinib for 30–150 min in SUM-149 (green line), MCF-10A + EGF (blue line) and MCF-10A + AREG cells (black line). The *Y*-axis shows normalized log2 values of fluorescence intensity for each antibody. See Supplemental Methods for details of the RPPA data analysis. †$P < 0.001$ by ANOVA of time series compared to MCF-10A + EGF; ‡$P < 0.001$ by ANOVA of time series compared to MCF-10A + AREG. B. SUM-149 cells expressing a Wnt-reporter construct cultured under 2D conditions. Representative images (left) and flow-cytometry analysis (right) of GFP-positive cells are shown. Scale bars = 400 μm. C. SUM-149 cells expressing a Wnt-reporter construct cultured in low-attachment plates in stem cell media. Representative images (left) and flow-cytometry analysis (right) of GFP-positive cells are shown. Scale bars = 400 μm.

Benjamini–Hochberg false discovery rate were identified. The results of this analysis demonstrated that in MCF-10A cells cultured in the presence of EGF, the expression of 1477 genes were altered following inhibition of EGFR, whereas in MCF-10A cells cultured in the continuous presence of AREG, only 258 genes were significantly altered in expression by EGFR inhibition. Gene ontology analysis of the genes altered in MCF-10A + EGF cells showed that the overwhelming majority of these genes were associated with mitosis, mitotic cell cycle, cell cycle progression, and processes associated with cell cycle regulation (Table 1, Supplementary Table 1). Similarly, genes that were altered in expression by inhibition of EGFR in MCF-10A + AREG cells were also exclusively associated with processes involved in cell cycle progression, cell division, M-

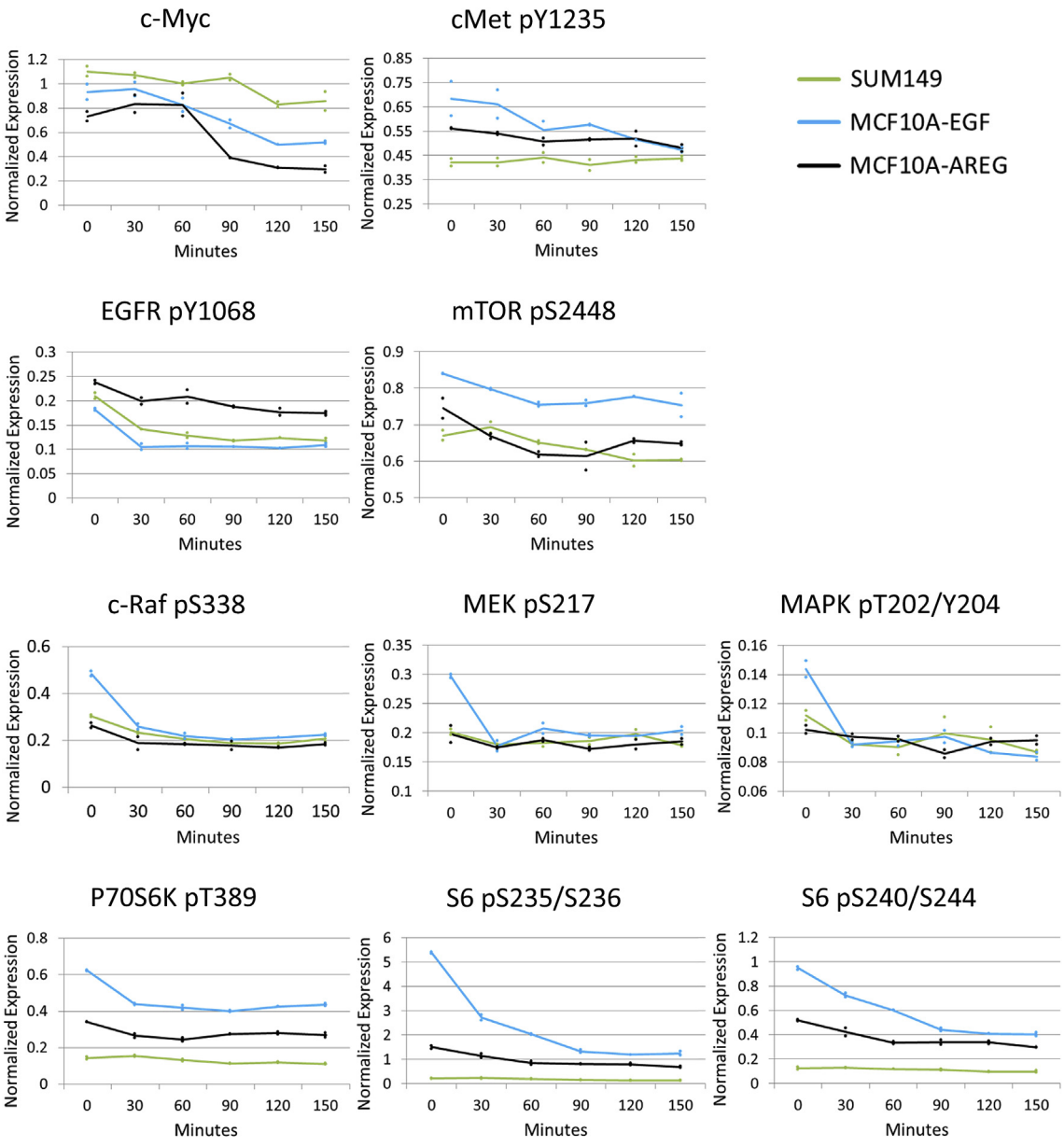

Figure 4 – Expression or phosphorylation of proteins in SUM-149, MCF-10A + EGF and MCF-10A + AREG cells following inhibition of EGFR by 0.5 μM gefitinib for 0, 30, 60, 90, 120, and 150 min.

phase, and related cell cycles processes (Table 2, Supplementary Table 2), and there was a large overlap in the cell cycle-associated genes regulated by EGFR regardless of the ligand.

We also performed RNA-Seq-based gene expression profiling on SUM-149 cells in the presence or absence of gefitinib. The expression of 226 genes in SUM-149 cells were statistically significantly altered following exposure to gefitinib, and these genes were associated with epithelial development, response to extracellular stimuli and metabolic processes (Table 3, Supplementary Table 3). Interestingly, many of the cell cycle and M-phase associated genes that were found to be altered by inhibition of EGFR in MCF-10A cells in the presence of either EGF or AREG were not affected by EGFR inhibition in SUM-149 cells. These findings indicate that the expression of a substantial number of genes is uncoupled from EGFR signaling in SUM-149 cells compared to MCF-10A cells.

3.4. *Functional analysis of gene expression using genome-scale shRNA screening*

The gene expression profiling studies described above yielded information that shed light on the biological effects of EGFR signaling in a ligand- and cell type-specific fashion. To explore the functional significance of the EGFR-associated gene expression profiles obtained from MCF-10A cells and SUM-149 cells, we performed genome-scale shRNA screening in both cell lines. The goal of these experiments was to identify genes necessary for growth and survival in these cell lines,

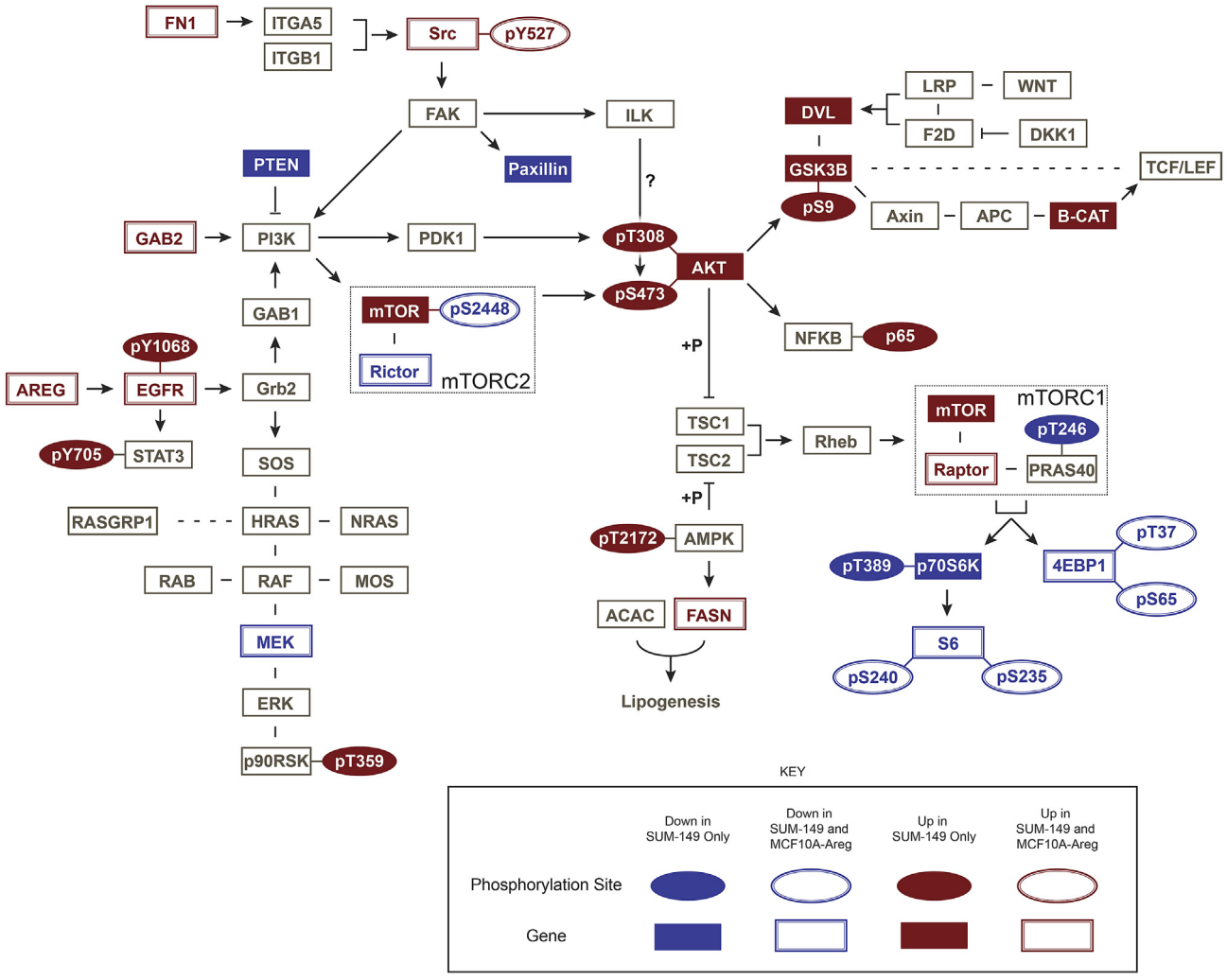

Figure 5 – Summary of results of RPPA analysis of EGFR signaling in MCF-10A + EGF, MCF-10A + AREG and SUM-149 cells. AREG-mediated activation of EGFR induces a dramatic up-regulation of FN1 expression and reduced expression and activation of proteins in the mTORC1 pathway. In addition, AREG-mediated EGFR activity in the context of PTEN loss results in higher levels of AKT phosphorylation, as well as changes in components of the Wnt/beta-catenin signaling pathway and NF-κB phosphorylation.

and to integrate that analysis with the analysis of genes that were altered in expression by inhibition of EGFR. To perform these experiments, MCF-10A or SUM-149 cells were transduced with a library of 82,000 lentiviral vectors expressing shRNAs targeting 15,377 cellular genes, with a minimum of four shRNAs per gene. Cells transduced with this library were harvested at day 3 after selection and again after approximately 7 population doublings. The abundance of shRNAs at both time points was determined by next-generation sequencing of PCR-amplified shRNA-associated barcodes. Fold-depletion values were then calculated by comparing the abundance of each shRNA at the final time point with the abundance at the initial time point.

To identify hits in the screen in a statistically robust manner, quant-log scores based on the fold-depletion values for each shRNA were determined for each gene targeted by shRNAs in the library (Figure 6A–D; see Methods and Supplementary Methods for details). A null distribution was generated based on the median value of the depletion scores for all shRNAs, and hits in the screen were determined as genes having quant log scores greater than the 95th percentile of the null distribution. Analysis of both positive and negative reference gene sets showed that this cut-off resulted in a very low rate of false-positives, while at the same time achieving a high true-positive rate. Using this method, we identified 1091 hits in the MCF-10A shRNA screen and 1052 hits in the SUM-149 screen. For an initial analysis of the screen hits in the two cell lines, we used Pathway Guide to examine the KEGG pathways that were statistically significantly enriched by the hit data from each line. The results of this analysis demonstrated a high degree of similarity in the canonical pathways containing hit genes in the two cell lines. Table 4 shows the top cancer-relevant pathways identified by the screen. Note that only pathways that achieved a pFDR of <0.05 in at least

Table 1 – Biological process gene annotation analysis of genes regulated by EGFR in MCF10A + EGF cells.

Biological process	Bonferroni *P*-value
M phase of mitotic cell cycle	<2.17E-40
Mitotic cell cycle	<2.17E-40
M phase	<2.17E-40
Nuclear division	<2.17E-40
Mitosis	<2.17E-40
Cell cycle phase	<2.17E-40
Organelle fission	<2.17E-40
Cell division	2.17E-40
Microtubule-based process	4.59E-23
Mitotic prometaphase	2.22E-22
Regulation of cell cycle	3.42E-22
Chromosome segregation	1.44E-21
Microtubule cytoskeleton organization	2.10E-21
Regulation of cell cycle process	5.14E-21
Regulation of organelle organization	5.59E-16
Spindle organization	6.94E-16
Cytoskeleton organization	5.85E-15
Regulation of mitotic cell cycle	1.43E-14
Sister chromatid segregation	4.21E-13
Mitotic sister chromatid segregation	4.59E-12

one of the cell lines are shown. As can be seen from Table 4, there was substantial overlap among the KEGG pathways identified using the screen hit data. Interestingly, while the Cell Cycle KEGG pathway was significantly enriched in both cell lines, many more hit genes mapped to this pathway in SUM-149 cells (29 vs. 13) than MCF-10A cells (Supplementary Figure 4). This result suggests that SUM-149 cells are more vulnerable to perturbations in genes that regulate the cell cycle, particularly mitotic progression, than are MCF-10A cells. In addition, the Wnt pathway was statistically significantly

Table 2 – Biological process gene annotation analysis of genes regulated by EGFR in MCF10A + AREG cells.

Biological process	Bonferroni *P*-value
Cell cycle	3.40E-78
M phase	2.00E-73
Cell cycle phase	5.10E-72
Cell cycle process	3.10E-69
Nuclear division	2.10E-66
Mitosis	2.10E-66
M phase of mitotic cell cycle	6.70E-66
Organelle fission	3.00E-65
Mitotic cell cycle	7.00E-64
Cell division	1.80E-54
Chromosome segregation	1.90E-30
Microtubule based process	6.40E-25
DNA metabolic process	5.60E-22
Regulation of cell cycle	1.10E-21
DNA replication	2.90E-21
Microtubule cytoskeleton organization	1.30E-18
Regulation of cell cycle process	9.80E-18
Regulation of mitotic cell cycle	4.10E-17
Mitotic sister chromatid segregation	1.10E-16
Spindle organization	1.60E-01

Table 3 – Biological process gene annotation analysis of genes regulated by EGFR in SUM-149 cells.

Biological process	Bonferroni *P*-value
Response to oxygen-containing compound	5.73E-35
Regulation of protein phosphorylation	5.28E-33
Regulation of protein modification process	6.68E-33
Response to organic cyclic compound	9.96E-33
Regulation of cell cycle	1.03E-32
Regulation of phosphorylation	1.04E-32
Enzyme linked receptor protein signaling pathway	4.85E-32
Purine ribonucleotide metabolic process	1.47E-31
Response to abiotic stimulus	1.84E-31
Ribonucleotide metabolic process	5.68E-31
Ribose phosphate metabolic process	1.05E-30
Response to organic nitrogen	1.39E-30
Response to nitrogen compound	3.59E-30
Purine-containing compound metabolic process	3.91E-30
Purine nucleotide metabolic process	5.72E-30
Regulation of protein kinase activity	3.61E-29
Regulation of kinase activity	4.47E-28
Purine ribonucleoside metabolic process	7.80E-28
Purine nucleoside metabolic process	9.72E-28
Transmembrane receptor protein tyrosine kinase signaling pathway	1.89E-27

enriched in SUM-149 cells but not MCF-10A cells, consistent with results described in the previous section. By contrast, the PI3K-AKT pathway was highly significant in MCF-10A cells, whereas it fell just below the significance threshold in SUM-149 cells (23 hit genes versus 16). Despite the pFDR value of the overall pathway falling above the 0.05 threshold for significance (pFDR = 0.078 for SUM-149 cells), two genes from the pathway were hits in the SUM-149 screen that were not hits in MCF-10A cells; ITGB1, which encodes integrin β1, and PIK3R2, which encodes the regulatory subunit β of PI3K. The finding of ITGB1 as a hit is consistent with results discussed above regarding the importance of fibronectin signaling in SUM-149 cells, and the PIK3R2 finding points to a predominant role for the p85β regulatory subunit of PI3K in these cells. These results were validated in separate experiments utilizing siRNA-mediated knockdown of these proteins in SUM-149 cells (Supplementary Figure 5).

We next compared the lists of genes that were hits in the screen with the lists of genes affected by inhibition of EGFR. Of the 1477 genes altered in expression by inhibition of EGFR in MCF-10A + EGF cells, 121 were hits in the SUM-149 screen (53 of these were also hits in the MCF10A shRNA screen). Only three of these genes, however, were regulated by EGFR in SUM-149 cells. Therefore, using this method, we identified 118 genes that were altered in expression by inhibition of EGFR in MCF-10A + EGF cells but uncoupled from regulation by EGFR in SUM-149 cells, and were also hits in the SUM-149 shRNA screen. The data for the top 20 of these genes are shown in Table 5, and the complete list of 121 genes is shown in Supplementary Table 4. Gene annotation analysis of the 118 EGFR-uncoupled genes that were hits in the SUM-149 screen showed that they map to categories associated with mitosis, cell division and cell cycle progression (Table 6). Thus, SUM-149 cells differ from MCF-10A cells in EGFR-mediated

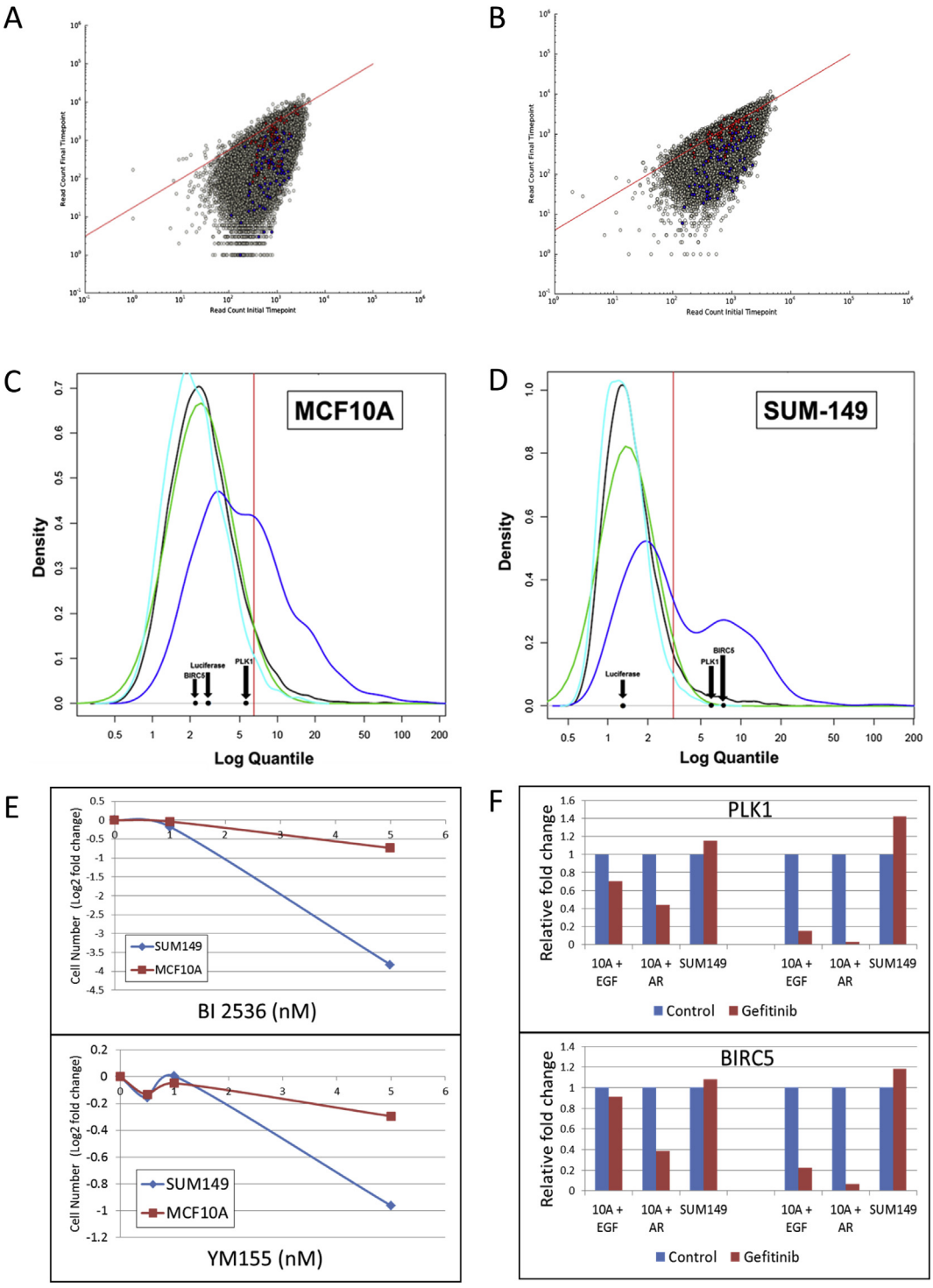

Figure 6 – Genome-scale shRNA screen of MCF-10A and SUM-149 cells. A,B. Scatter plots were generated using initial and final time point read counts for each shRNA in the genome-wide screen in MCF10A (A) and SUM-149 (B) cells. Red data points indicate shRNAs targeting Luciferase, which served as a negative control, while blue data points indicate shRNAs targeting EIF3A, which served as a positive control. In both plots, a solid line with a *y*-intercept of 3 and a slope of 1 was plotted as a reference. C,D. Log quantile scores calculated for each gene in the genome-wide shRNA screens in MCF-10A (A) and SUM-149 (B) cells were used to generate probability density plots. The black (—) plot was generated using scores for all genes, the blue (—) plot using scores for commonly essential genes as defined by Moffat et al. (Koh et al., 2012), the turquoise (—) plot using scores for the negative control gene set, and the green (—) plot is a normal distribution determined by the median of the scores for all genes. The red line indicates the 95th percentile of the normal distribution used as a cutoff for determining hits in each screen. Black arrows indicate the quant log scores for Luciferase, PLK1 and BIRC5 in each cell line. E. Growth assays of MCF-10A and SUM-149 cells treated for 7 days with inhibitors of PLK1 (BI 2536, 0–5 nM, upper panel) and BIRC5 (YM155, 0–5 nM, lower panel). F. mRNA levels of PLK1 (upper panel) and BIRC5 (lower panel) in MCF-10A and SUM-149 cells following treatment with 0.5 μM gefitinib for 24 h. Graphs show results from two representative assays.

Table 4 – Top cancer relevant KEGG canonical pathways enriched by hits in genome-wide shRNA screening.

Pathway	SUM-149				MCF10A			
	pSize	No. Hits	P-Value	FDR	pSize	No. Hits	P-Value	FDR
Cell cycle	124	21	0.000000	0.000141	124	9	0.000790	0.009314
Pathways in cancer	327	19	0.000006	0.000490	327	12	0.029301	0.180254
Insulin signaling pathway	140	10	0.000182	0.001051	140	9	0.001850	0.028280
ErbB signaling pathway	88	7	0.000884	0.002408	88	7	0.001754	0.031233
TGF-beta signaling pathway	81	6	0.002934	0.003925	81	7	0.001081	0.021957
Wnt signaling pathway	143	10	0.000216	0.008248	143	8	0.007458	0.102847
Focal adhesion	206	11	0.001053	0.015033	206	16	0.000004	0.001079
PI3K-Akt signaling pathway	347	13	0.008438	0.063974	347	20	0.000022	0.001681

pSize indicates the number of genes in the KEGG pathway.
No. Hits indicates the number of significant hits in the shRNA screen.
P-Value indicates the probability of obtaining the number of screen hits in the pathway by chance alone.
FDR indicates the global probability corrected for false discovery rate of obtaining the indicated number of pathway hits by chance alone.

regulation of genes essential for mitosis and cell cycle progression and that are essential for the growth and survival of SUM-149 cells. Two genes in this list, BIRC5 (survivin) and PLK1 (Polo-like kinase 1), are of particular interest because their expression was strongly influenced by EGFR in MCF-10A cells, but were not gefitinib-sensitive in SUM-149 cells, and this finding was also confirmed in separate experiments by transient transfection with siRNAs (Supplementary Figure 5). BIRC5 is a well-known inhibitor of apoptosis in breast cancer cells (Jha et al., 2012) and PLK1 has recently been identified as a potential therapeutic target in TNBC cells (Maire et al., 2013). In addition, COLT analysis of essential genes in 29 breast cancer lines identified BIRC5 as a hit in 14 (48%) and PLK1 as a hit in 27 (93%) of these lines, including MDA-MB-468 and MDA-MB-231, both of which express high levels of EGFR (Koh et al., 2012). Treatment of SUM-149 cells with pharmacological inhibitors of BIRC5 or PLK1 resulted in a dramatic decrease in cell viability and demonstrated that SUM-149 cells were more sensitive to these drugs than MCF-10A cells (Figure 6F). In addition, qRT-PCR analysis confirmed that inhibition of EGFR with gefitinib results in decreased expression of BIRC5 and PLK-1 in MCF10A cells, but not SUM-149 cells (Figure 6E). The results of this shRNA screening experiment combined with our analysis of changes in gene expression resulting from inhibition of EGFR suggests that uncoupling of the genes that play key roles in cell survival from regulation by EGFR is part of the mechanism by which these breast cancer cells survive under conditions of prolonged EGFR inhibition. This finding could explain why EGFR

Table 5 – Top 20 genes uncoupled from EGFR regulation in SUM-149 cells.

Gene symbol	Log2 Fold Change[a]	MCF10A screen hit	SUM149 screen hit	P-Value
PLK1	−2.17	No	**Yes**	1.26E-15
DUSP6	−3.46	No	**Yes**	4.55E-15
IARS	−1.98	**Yes**	**Yes**	2.00E-14
PSCA	2.41	No	**Yes**	2.21E-14
NUF2	−2.49	**Yes**	**Yes**	9.30E-14
CLDN8	2.77	No	**Yes**	2.21E-13
RANGAP1	−1.52	No	**Yes**	1.28E-10
BIRC5	−1.75	No	**Yes**	3.09E-09
KIF11	−1.50	No	**Yes**	1.37E-08
DDX21	−1.17	**Yes**	**Yes**	1.75E-08
TCOF1	−1.55	No	**Yes**	3.14E-08
NCAPH	−1.76	**Yes**	**Yes**	5.31E-08
MARS	−2.14	**Yes**	**Yes**	5.40E-08
PFDN2	−1.60	**Yes**	**Yes**	6.45E-08
LARS	−1.06	**Yes**	**Yes**	1.21E-07
MTHFD1L	−1.75	No	**Yes**	1.71E-07
PRKCD	1.15	No	**Yes**	1.74E-07
TUBA1C	−1.16	No	**Yes**	2.60E-07
HSPA9	−1.15	No	**Yes**	2.98E-07
CKAP5	−1.02	**Yes**	**Yes**	6.46E-07

a Log2 Fold Change in MCF10A + EGF cells treated with 0.5 μM gefitinib for 24 h.

Table 6 – Biological processes associated with genes uncoupled from EGFR regulation in SUM-149 cells.

GO term	Count	%	P-Value
Mitotic cell cycle	20	16.9	5.40E-11
Cell division	18	15.3	1.00E-10
Nuclear division	16	13.6	1.40E-10
Mitosis	16	13.6	1.40E-10
M phase of mitotic cell cycle	16	13.6	1.80E-10
Organelle fission	16	13.6	2.50E-10
Cell cycle process	22	18.6	1.80E-09
Cell cycle phase	19	16.1	2.70E-09
M phase	17	14.4	4.60E-09
Cell cycle	24	20.3	2.00E-08
ncRNA metabolic process	14	11.9	2.50E-08
tRNA aminoacylation for protein translation	8	6.8	5.80E-08
Amino acid activation	8	6.8	5.80E-08
tRNA aminoacylation	8	6.8	5.80E-08
Ribonucleoprotein complex biogenesis	11	9.3	1.30E-06
tRNA metabolic process	8	6.8	3.60E-05
Chromosome segregation	7	5.9	3.80E-05
Ribosome biogenesis	8	6.8	4.50E-05
RNA processing	14	11.9	3.10E-04
Spindle organization	5	4.2	4.00E-04

inhibitors have been relatively ineffective in breast cancer clinical trials.

4. Discussion

TNBCs are distinct from other breast cancer types in that they do not have a single dominant driver of tumorigenicity. Thus, these breast cancers are unlike breast cancers driven by the estrogen receptor (ER) or HER-2 oncogene. The lack of a distinct driver of malignancy in this subset of cancers has hampered efforts to develop targeted drugs that are effective in this setting. Recent work from our laboratory and other groups using cell line models of TNBC suggests that these breast cancers rely on the combined action of multiple drivers, which together form an oncogenic signaling network that functions in a manner similar to classical dominant driving oncogenes. In the work reported here, we show that a subset of TNBC cells with cell surface accumulation, stabilization and constitutive activation of EGFR have an oncogenic signaling network characterized by PTEN loss and consequent dysregulated PI3′K signaling. The working model developed from the results reported here predicts that the combined action of these events drives unregulated cell proliferation as well as motility and invasion. The model also points to regions of vulnerability in the oncogenic signaling network that predict combinatorial drug strategies that could disable the network in a manner that would have a large effect on the viability of the cancer cells.

We showed previously that an important aspect of the biology of AREG is how it affects the trafficking and stability of EGFR. AREG-stimulated EGFR has a long half-life compared to EGF-stimulated EGFR, and is either stabilized or recycled to the cell surface, resulting in overexpression of EGFR at the protein level (Willmarth et al., 2008). This observation has been confirmed by others (Busser et al., 2011; Roepstorff et al., 2009). The overexpression of cell surface-associated EGFR is consistent with a long-standing body of data that indicates that overexpression of EGFR at the protein level is associated with aggressive disease and poor prognosis in breast cancer (Harris et al., 1989; Nicholson et al., 1989, 1990, 1991; Kancha et al., 2009).

In the present work, we found that AREG-stimulated EGFR affects cell signaling and gene expression in a manner distinct from that of EGF-stimulated EGFR in the same cell line. This result suggests that the changes in the stability and trafficking of EGFR activated by AREG have important downstream effects. One of the key genes altered in expression by AREG compared to EGF is FN1. mRNA levels of fibronectin were increased nearly 20-fold in MCF-10A + AREG cells, and FN1 mRNA levels were also higher in SUM-149 cells compared to EGF-stimulated MCF-10A cells. Similarly, high levels of FN1 mRNA and protein were observed in SUM-229 cells, which also express high levels of AREG and are PTEN null. We reported previously that AREG-stimulated activation of EGFR results in the acquisition of motile and invasive phenotypes in MCF-10A cells and that knock-down of AREG in SUM-149 cells significantly reduces their motile and invasive properties (Baillo et al., 2011; Willmarth and Ethier, 2006). In addition, the high level of AKT pS473 is particularly interesting given the increase in FN1 protein expression observed in these cells. α5β1 integrin is the fibronectin receptor, and β1 integrin signaling has been reported to activate mTORC2 activity in a PI3′K-dependent manner (Zeller et al., 2010). In addition, the gene that encodes integrin β1 was a hit in the shRNA screen. These results suggest that high levels of β1 integrin signaling induced by FN1 overexpression, coupled with the PTEN loss, results in dramatic elevation of PI3′K-activated AKT levels in SUM-149 cells. While these results also suggest that mTORC2 is the PDK2 active in SUM-149 cells, it remains possible that other kinases, such as integrin-linked kinase (ILK), can mediate or participate in phosphorylation of AKT pS473 in these cells (Riaz et al., 2012; Lee et al., 2013). Indeed, ILK was a hit in the shRNA screen in SUM-149 cells. Overall, the present results point to regulation of FN1 as a major mediator of the phenotype of these cells, and, other work from our laboratory, as well as that of our collaborators, clearly demonstrate the important role of fibronectin-mediated integrin signaling in the invasive potential of breast, prostate and lung cancer cells (Jia et al., 2004; Livant et al., 1995; Livant et al., 2000).

Our results also point to a potent interaction between oncogenic signaling by EGFR and the loss of regulation of PI3′K that results from PTEN loss. This combination of factors has been repeatedly observed in clinical TNBC specimens and several cell line models, including SUM-149 and SUM-229 cells (Lehmann et al., 2011; Martin et al., 2012). MDA-MB-468 cells also have an EGFR gene amplification resulting in overexpression and cell surface accumulation of EGFR protein, and these cells are also PTEN null. Pires et al. (2013) recently demonstrated the profound transforming ability of EGFR overexpression coupled with PTEN loss and p53 mutation in immortalized human mammary epithelial cells. In our experiments, the loss of PTEN in the context of constitutive EGFR oncogenic signaling had profound effects on downstream signaling and gene expression. SUM-149 cells exhibited increased levels of AKT protein and dramatically increased levels of phosphorylated AKT at both the pT308 and pS473 sites that was independent of EGFR activity. SUM-149 cells also exhibit elevated levels of Dvl protein and GSK3β phosphorylation, changes that have been shown to result in the stabilization of beta-catenin, which is required for canonical Wnt signaling. In addition, we demonstrated previously that AREG-mediated EGFR signaling influences the Wnt pathway by transcriptionally down-regulating the expression of DKK1 and SFRP1, two negative regulators of Wnt activity (Baillo et al., 2011). Given the increased expression/phosphorylation of Wnt pathway mediators revealed by RPPA analysis in SUM-149 cells compared to MCF-10A cells, and that GSK3β is a known AKT substrate, one could hypothesize that this high level constitutive AKT activation in a PTEN null background poises the cells for Wnt/beta-catenin signaling and hence self-renewal. Indeed, we found that when cultured under anchorage-independent conditions, SUM-149 cells exhibited Wnt/beta-catenin activity, and exhibited distinct clusters of TCF/LEF-positive cells when cultured in low-attachment plates in stem cell media. Further work will be required to confirm the link between oncogenic EGFR signaling and PTEN loss and the activation of Wnt signaling in these cells.

In these studies, we identified a set of genes that were transcriptionally regulated by EGFR in MCF-10A cells but were uncoupled from EGFR activity in SUM-149 cells. Once again, it is likely that the loss of PTEN plays a role in this uncoupling of gene expression, since AKT activation was not affected by gefitinib in these cells. What makes this observation especially intriguing, however, is the finding that many of these EGFR-uncoupled genes were strong hits in the shRNA screens, particularly the SUM-149 screen. This is a potentially important observation, as it may explain why EGFR signaling is required for survival of MCF-10A cells but not SUM-149 cells. We have known for many years that exposure of SUM-149 cells to gefitinib for extended periods results in complete cell cycle arrest, and that this effect is fully reversible for both monolayer growth and colony forming efficiency (Rao et al., 2000). Thus, EGFR is important for the proliferation of SUM-149 cells, but not for their viability. The current results show that key survival genes, such as BIRC5 and PLK1, remain expressed at normal levels in gefitinib-treated SUM-149 cells, but are dramatically decreased in expression in gefitinib treated MCF-10A cells. And, these genes were strong hits in the SUM-149 screen, indicating that they are required for growth/survival of these cells. Furthermore, these genes are but two in a large set of EGFR-uncoupled genes that were found to essential for growth/survival in the SUM-149 shRNA screen. Thus, the uncoupling of regulation of these genes from the EGFR in SUM-149 cells is likely to play a role in their survival in the presence of EGFR inhibition. If this uncoupling is the result of the AREG-EGFR-PTEN-null oncogenic signaling network that is common in TNBC cells, it could explain why EGFR inhibitors have been ineffective in patients with this type of breast cancer. In EGFR mutation-positive non-small cell lung cancer cells, BIRC5 expression in PTEN-null variants was also unaffected by treatment with the EGFR-TKI inhibitor, erlotinib, in contrast to the parental PTEN-competent cells (Okamoto et al., 2012). In addition, PTEN-null prostate cancer cells were more sensitive to inhibition of PLK-1 than PTEN-expressing cells (Liu et al., 2011). In that regard, our model makes specific predictions as to how combinations of targeted inhibitors could be employed to inactivate the oncogenic signaling network in these cells. For example, targeting PLK1 and/or BIRC5 directly while inhibiting EGFR signaling could serve to re-couple these key proteins and affect cell survival. Similarly, identification of the kinase responsible for AKT pS473 (mTORC2 versus ILK, for example) could identify a mechanism by which to specifically inactivate the increased AKT signaling that occurs in the PTEN null background, and may also be used in combination with EGFR inhibitors to re-couple expression of key survival genes. Finally, Livant and co-workers have developed potent inhibitors of fibronectin-mediated integrin signaling, which have been found to be highly effective in pre-clinical models, and have been confirmed to be safe for therapeutic administration in Phase I clinical trials (Yao et al., 2011; Veine et al., 2014). These drugs could be combined with other targeted inhibitors to completely inactivate the oncogenic signaling network active in this subset of TNBC cells.

In summary, our results point to the presence of an oncogenic signaling network in a subset of TNBC cells that is characterized by constitutive cell surface-associated EGFR signaling coupled to PTEN loss, which together drives fibronectin-mediated integrin signaling and may also be responsible for Wnt/beta-catenin and NF-κB activity in these cells. The model that we have derived from these findings, coupled with our previously published data, suggest that this oncogenic signaling network plays a direct role not only in driving growth factor-independent proliferation and survival of these breast cancer cells, but also regulates their motility/invasion, their self-renewal potential via Wnt/beta-catenin activity, and their intrinsic drug resistance, possibly via NF-κB activation. Importantly, this model makes specific predictions for combinatorial strategies using targeted inhibitors to inactivate the network and impact the growth and survival of these breast cancer cells.

Conflicts of interest

The authors have no conflicts of interest to declare.

Acknowledgments

We would like to thank Jennifer Schulte, Danielle Woodford, Ericka Smith and Carlene Brandon for their technical assistance. Bioinformatics analysis was performed by Gerard T. Hardiman at the CGM Bioinformatics Core at MUSC. RPPA analysis was performed by the MD Anderson RPPA Core Facility (funded by National Cancer Institute # CA16672). This work was supported in part by the Cell Evaluation & Therapy Shared Resource (P30 CA138313) and Genomics Shared Resource Facilities, Hollings Cancer Center, Medical University of South Carolina. This work was funded by a grant from the National Institutes of Health National Cancer Institute R01CA130933.

Appendix A. Supplementary data

Supplementary data related to this article can be found at http://dx.doi.org/10.1016/j.molonc.2014.10.006.

REFERENCES

Agrawal, A., Gutteridge, E., Gee, J.M., Nicholson, R.I., Robertson, J.F., 2005. Overview of tyrosine kinase inhibitors in clinical breast cancer. Endocr. Relat. Cancer 12 (Suppl. 1), S135–S144.

Baillo, A., Giroux, C., Ethier, S.P., 2011. Knock-down of amphiregulin inhibits cellular invasion in inflammatory breast cancer. J. Cell Physiol. 226 (10), 2691–2701.

Beerli, R.R., Hynes, N.E., 1996. Epidermal growth factor-related peptides activate distinct subsets of ErbB receptors and differ in their biological activities. J. Biol. Chem. 271 (11), 6071–6076.

Berquin, I.M., Dziubinski, M.L., Nolan, G.P., Ethier, S.P., 2001. A functional screen for genes inducing epidermal growth factor autonomy of human mammary epithelial cells confirms the role of amphiregulin. Oncogene 20, 4019–4028.

Buick, R.N., Filmus, J., Church, J., 1990. Studies of EGF-mediated growth control and signal transduction using the MDA-MB-

468 human breast cancer cell line. Prog. Clin. Biol. Res. 354A, 179–191.
Busser, B., Sancey, L., Brambilla, E., Coll, J.L., Hurbin, A., 2011. The multiple roles of amphiregulin in human cancer. Biochim. Biophys. Acta 1816 (2), 119–131.
Dahiya, N., Becker, K.G., Wood 3rd, W.H., Zhang, Y., Morin, P.J., 2011. Claudin-7 is frequently overexpressed in ovarian cancer and promotes invasion. PLoS One 6 (7), e22119.
Danielsen, A.J., Maihle, N.J., 2002. The EGF/ErbB receptor family and apoptosis. Growth Factors 20 (1), 1–15.
Ding, L., Lu, Z., Lu, Q., Chen, Y.H., 2013. The claudin family of proteins in human malignancy: a clinical perspective. Cancer Manag. Res. 5, 367–375.
Ethier, S.P., 1996. Human breast cancer cell lines as models of growth regulation and disease progression. J. Mammary Gland Biol. Neoplasia 1 (1), 111–121.
Ethier, S.P., Mahacek, M.L., Gullick, W.J., Frank, T.J., Weber, B.L., 1993. Differential isolation of normal luminal mammary epithelial cells and breast cancer cells from primary and metastatic sites using selective media. Cancer Res. 53, 627–635.
Ethier, S.P., Kokeny, K.E., Ridings, J.E., Dilts, C.A., 1996. erbB family receptor expression and growth regulation in a newly isolated human breast cancer cell line. Cancer Res. 56, 899–907.
Forozan, F., Veldman, R., Ammerman, C.A., Parsa, N.Z., Kallioniemi, A., Kallioniemi, O., Ethier, S.P., 1999. Molecular cytogenetic analysis of 11 new human breast cancer cell lines. Br. J. Cancer 81 (8), 1328–1334.
Fuerer, C., Nusse, R., 2010. Lentiviral vectors to probe and manipulate the Wnt signaling pathway. PLoS One 5 (2), e9370.
Harris, A.L., Nicholson, S., Sainsbury, J.R.C., Farndon, J., Wright, C., 1989. Epidermal growth factor receptors in breast cancer: association with early relapse and death, poor response to hormones and interactions with neu. J. Steroid Biochem. 34, 123–131.
Jha, K., Shukla, M., Pandey, M., 2012. Survivin expression and targeting in breast cancer. Surg. Oncol. 21 (2), 125–131.
Jia, Y., Zeng, Z.Z., Markwart, S.M., Rockwood, K.F., Ignatoski, K.M., Ethier, S.P., Livant, D.L., 2004. Integrin fibronectin receptors in matrix metalloproteinase-1-dependent invasion by breast cancer and mammary epithelial cells. Cancer Res. 64 (23), 8674–8681.
Johnson, G.R., Wong, L., 1994. Heparan sulfate is essential to amphiregulin-induced mitogenic signaling by the epidermal growth factor receptor. J. Biol. Chem. 269 (43), 27149–27154.
Johnson, G.R., Kannan, B., Shoyab, M., Stromberg, K., 1993. Amphiregulin induces tyrosine phosphorylation of the epidermal growth factor receptor and p185(erbB2) – evidence that amphiregulin acts exclusively through the epidermal growth factor receptor at the surface of human epithelial cells. J. Biol. Chem. 268 (4), 2924–2931.
Kancha, R.K., von Bubnoff, N., Peschel, C., Duyster, J., 2009. Functional analysis of epidermal growth factor receptor (EGFR) mutations and potential implications for EGFR targeted therapy. Clin. Cancer Res. 15 (2), 460–467.
Katoh, M., Igarashi, M., Fukuda, H., Nakagama, H., Katoh, M., 2013. Cancer genetics and genomics of human FOX family genes. Cancer Lett. 328 (2), 198–206.
Koh, J.L., Brown, K.R., Sayad, A., Kasimer, D., Ketela, T., Moffat, J., 2012. COLT-Cancer: functional genetic screening resource for essential genes in human cancer cell lines. Nucleic Acids Res. 40 (Database issue), D957–D963.
Lee, S.L., Chou, C.C., Chuang, H.C., Hsu, E.C., Chiu, P.C., Kulp, S.K., Byrd, J.C., Chen, C.S., 2013. Functional role of mTORC2 versus integrin-linked kinase in mediating Ser473-Akt phosphorylation in PTEN-negative prostate and breast cancer cell lines. PLoS One 8 (6), e67149.
Lehmann, B.D., Bauer, J.A., Chen, X., Sanders, M.E., Chakravarthy, A.B., Shyr, Y., Pietenpol, J.A., 2011. Identification of human triple-negative breast cancer subtypes and preclinical models for selection of targeted therapies. J. Clin. Invest. 121 (7), 2750–2767.
Liu, X.S., Song, B., Elzey, B.D., Ratliff, T.L., Konieczny, S.F., Cheng, L., Ahmad, N., Liu, X., 2011. Polo-like kinase 1 facilitates loss of Pten tumor suppressor-induced prostate cancer formation. J. Biol. Chem. 286 (41), 35795–35800.
Livant, D.L., Linn, S., Markwart, S., Shuster, J., 1995. Invasion of selectively permeable sea urchin embryo basement membranes by metastatic tumor cells, but not by their normal counterparts. Cancer Res. 55, 5085–5093.
Livant, D.L., Brabec, R.K., Pienta, K.J., Allen, D.L., Kurachi, K., Markwart, S., Upadhyaya, A., 2000. Anti-invasive, antitumorigenic, and antimetastatic activities of the PHSCN sequence in prostate carcinoma. Cancer Res. 60 (2), 309–320.
Ma, L., de Roquancourt, A., Bertheau, P., Chevret, S., Millot, G., Sastre-Garau, X., Espie, M., Marty, M., Janin, A., Calvo, F., 2001. Expression of amphiregulin and epidermal growth factor receptor in human breast cancer: analysis of autocriny and stromal-epithelial interactions. J. Pathol. 194 (4), 413–419.
Maire, V., Nemati, F., Richardson, M., Vincent-Salomon, A., Tesson, B., Rigaill, G., Gravier, E., Marty-Prouvost, B., De Koning, L., Lang, G., et al., 2013. Polo-like kinase 1: a potential therapeutic option in combination with conventional chemotherapy for the management of patients with triple-negative breast cancer. Cancer Res. 73 (2), 813–823.
Martin, V., Botta, F., Zanellato, E., Molinari, F., Crippa, S., Mazzucchelli, L., Frattini, M., 2012. Molecular characterization of EGFR and EGFR-downstream pathways in triple negative breast carcinomas with basal like features. Histol. Histopathol 27 (6), 785–792.
Masuda, H., Baggerly, K.A., Wang, Y., Zhang, Y., Gonzalez-Angulo, A.M., Meric-Bernstam, F., Valero, V., Lehmann, B.D., Pietenpol, J.A., Hortobagyi, G.N., et al., 2013. Differential response to neoadjuvant chemotherapy among 7 triple-negative breast cancer molecular subtypes. Clin. Cancer Res. 19 (19), 5533–5540.
Narita, K., Chien, J., Mullany, S.A., Staub, J., Qian, X., Lingle, W.L., Shridhar, V., 2007. Loss of HSulf-1 expression enhances autocrine signaling mediated by amphiregulin in breast cancer. J. Biol. Chem. 282 (19), 14413–14420.
Nicholson, S., Halcrow, P., Farndon, J.R., Sainsbury, J.R.C., Chambers, P., Harris, A.L., 1989. Expression of epidermal growth factor receptors associated with lack of response to endocrine therapy in recurrent breast cancer #151. Lancet (8631), 182–185.
Nicholson, S., Wright, C., Sainsbury, J.R., Halcrow, P., Kelly, P., Angus, B., Farndon, J.R., Harris, A.L., 1990. Epidermal growth factor receptor (EGFr) as a marker for poor prognosis in node-negative breast cancer patients: neu and tamoxifen failure #1738. J. Steroid Biochem. Mol. Biol. 37 (6), 811–814.
Nicholson, S., Richard, J., Sainsbury, C., Halcrow, P., Kelly, P., Angus, B., Wright, C., Henry, J., Farndon, J.R., Harris, A.L., 1991. Epidermal growth factor receptor (EGFr) – results of a six year follow-up study in operable breast cancer with emphasis on the node negative subgroup #401. Br. J. Cancer 63 (1), 146–150.
Okamoto, K., Okamoto, I., Hatashita, E., Kuwata, K., Yamaguchi, H., Kita, A., Yamanaka, K., Ono, M., Nakagawa, K., 2012. Overcoming erlotinib resistance in EGFR mutation-positive non-small cell lung cancer cells by targeting survivin. Mol. Cancer Ther. 11 (1), 204–213.
Pal, S.K., Childs, B.H., Pegram, M., 2011. Triple negative breast cancer: unmet medical needs. Breast Cancer Res. Treat. 125 (3), 627–636.
Pires, M.M., Hopkins, B.D., Saal, L.H., Parsons, R.E., 2013. Alterations of EGFR, p53 and PTEN that mimic changes found

in basal-like breast cancer promote transformation of human mammary epithelial cells. Cancer Biol. Ther. 14 (3), 246–253.
Prat, A., Perou, C.M., 2011. Deconstructing the molecular portraits of breast cancer. Mol. Oncol. 5 (1), 5–23.
Prat, A., Adamo, B., Cheang, M.C., Anders, C.K., Carey, L.A., Perou, C.M., 2013. Molecular characterization of basal-like and non-basal-like triple-negative breast cancer. Oncologist 18 (2), 123–133.
Rao, G.S., Murray, S., Ethier, S.P., 2000. Radiosensitization of human breast cancer cells by a novel ErbB family receptor tyrosine kinase inhibitor. Int. J. Radiat. Oncol. Biol. Phys. 48 (5), 1519–1528.
Riaz, A., Zeller, K.S., Johansson, S., 2012. Receptor-specific mechanisms regulate phosphorylation of AKT at Ser473: role of RICTOR in beta1 integrin-mediated cell survival. PLoS One 7 (2), e32081.
Roepstorff, K., Grandal, M.V., Henriksen, L., Knudsen, S.L., Lerdrup, M., Grovdal, L., Willumsen, B.M., van Deurs, B., 2009. Differential effects of EGFR ligands on endocytic sorting of the receptor. Traffic (Copenhagen, Denmark) 10 (8), 1115–1127.
Saal, L.H., Gruvberger-Saal, S.K., Persson, C., Lovgren, K., Jumppanen, M., Staaf, J., Jonsson, G., Pires, M.M., Maurer, M., Holm, K., et al., 2008. Recurrent gross mutations of the PTEN tumor suppressor gene in breast cancers with deficient DSB repair. Nat. Genet. 40 (1), 102–107.
Schneider, B.P., Winer, E.P., Foulkes, W.D., Garber, J., Perou, C.M., Richardson, A., Sledge, G.W., Carey, L.A., 2008. Triple-negative breast cancer: risk factors to potential targets. Clin. Cancer Res. 14 (24), 8010–8018.
Stern, K.A., Place, T.L., Lill, N.L., 2008. EGF and amphiregulin differentially regulate Cbl recruitment to endosomes and EGF receptor fate. Biochem. J. 410 (3), 585–594.
Streicher, K.L., Willmarth, N.E., Garcia, J., Boerner, J.L., Dewey, T.G., Ethier, S.P., 2007. Activation of a nuclear factor kappaB/interleukin-1 positive feedback loop by amphiregulin in human breast cancer cells. Mol. Cancer Res. 5 (8), 847–861.
Veine, D.M., Yao, H., Stafford, D.R., Fay, K.S., Livant, D.L., 2014. A D-amino acid containing peptide as a potent, noncovalent inhibitor of alpha5beta1 integrin in human prostate cancer invasion and lung colonization. Clin. Exp. Metastasis 31 (4), 379–393.
Willmarth, N.E., Ethier, S.P., 2006. Autocrine and juxtacrine effects of amphiregulin on the proliferative, invasive, and migratory properties of normal and neoplastic human mammary epithelial cells. J. Biol. Chem. 281 (49), 37728–37737.
Willmarth, N.E., Baillo, A., Dziubinski, M.L., Wilson, K., Riese 2nd, D.J., Ethier, S.P., 2008. Altered EGFR localization and degradation in human breast cancer cells with an amphiregulin/EGFR autocrine loop. Cell. Signal. 21 (2), 212–219.
Woods Ignatoski, K., Ethier, S.P., 1999. Constitutive activation of pp 125fak in eleven newly isolated breast cancer cell lines. Breast Cancer Res. Treat. 54, 173–182.
Yang, C., Chen, H., Yu, L., Shan, L., Xie, L., Hu, J., Chen, T., Tan, Y., 2013. Inhibition of FOXM1 transcription factor suppresses cell proliferation and tumor growth of breast cancer. Cancer Gene Ther. 20 (2), 117–124.
Yao, H., Veine, D.M., Fay, K.S., Staszewski, E.D., Zeng, Z.Z., Livant, D.L., 2011. The PHSCN dendrimer as a more potent inhibitor of human breast cancer cell invasion, extravasation, and lung colony formation. Breast Cancer Res. Treat. 125 (2), 363–375.
Zeller, K.S., Idevall-Hagren, O., Stefansson, A., Velling, T., Jackson, S.P., Downward, J., Tengholm, A., Johansson, S., 2010. PI3-kinase p110alpha mediates beta1 integrin-induced Akt activation and membrane protrusion during cell attachment and initial spreading. Cell. Signal. 22 (12), 1838–1848.